Presented at the 29th European PV Solar Energy Conference and Exhibition, 22-26 September 2014, Amsterdam, The Netherlands

PLATED NICKEL-COPPER CONTACTS ON C-SI: FROM MICROELECTRONIC PROCESSING TO COST EFFECTIVE SILICON SOLAR CELL PRODUCTION

Andrew Mondon*[1], Jonas Bartsch[1], Mathias Kamp[1], Andreas Brand[1], Bernd Steinhauser[1],Norbert Bay[2], Jörg Horzel[2], Markus Glatthaar[1], Stefan W. Glunz[1]
[1]Fraunhofer ISE, Heidenhofstr. 2, 79110 Freiburg, Germany
[2]Rena GmbH, Hans-Bunte-Str. 19, 79108 Freiburg, Germany

ABSTRACT: One of the key topics for industrial implementation of fully plated NiCu contacts on Si solar cells has so far been metal adhesion to silicon. The evaluation of adhesion is not entirely consistent throughout PV research, which is discussed at first. The adhesion issue of plated NiCu contacts has then been addressed by following two different routes for adhesion promotion. Firstly an "Interim Anneal" route is focussing on controlled silicide formation as a bonding agent and reliably excellent adhesion greater than wafer breakage force is shown independent of surface roughness (above 2 N/mm for measurements on clamped cells and above 4 N/mm for fortified wafers). Secondly a "Post Anneal" route is focussing on creation of high Si surface roughness by ps laser ablation of the ARC and annealing after full metallization. Excellent adhesion above wafer breakage force is demonstrated. Comparisons to different methods of ARC patterning and resulting surface roughness are made. The presented metallization technology is feasible for standard BSF cells and next generation solar cells for both p-type and n-type emitters. Solar cell efficiencies of up to 19.4%$_{abs}$ for p-type BSF cells, 20.5%$_{abs}$ for n-type BSF cells and 22.1%$_{abs}$ for n-type *PassDop* cells are presented.

Keywords: c-Si, Metallization, Plating, Fabrication, Laser Processing, Module Integration, Adhesion

1 INTRODUCTION

This contribution deals with direct nickel-silicon contacts on silicon solar cells as an alternative to silver screen printing as metallization of standard and next generation solar cells. Nickel based contacts on ps-laser patterns in the anti-reflection coating have been shown to be perfectly suitable for current industrial standard emitters and to even offer perspectives for advanced emitters [1]–[4]. The controlled formation of a silicide layer allows low resistivity contact formation, resulting in high efficiency solar cells [1], [4]–[8]. The complete metallization may be done by low cost wet chemical processes and low cost materials such as Cu may be applied. A plated Ni seed layer has been shown to hinder otherwise detrimental Cu penetration into the Si bulk well beyond typical module lifetimes [5][9]. Also a thin capping layer of Ag or Sn may be reliably applied electrochemically for corrosion resistance and enhanced solderability.

The first company to industrially implement plated NiCu contacts was BP-solar with their so-called "Saturn Cells" featuring "Laser Grooved Buried Contacts (LGBC)" in 1990 [5]. Modules from that time are still operational today, which can be seen as a proof of concept. However, too high process complexity and company internal issues led to abandonment of the process by BP in the mid-2000s. Another attempt to introduce NiCu technology was made by Suntech Power Holdings in 2009 with their high performance "Pluto Modules" [10]. Process complexity was greatly reduced by use of laser-doped selective emitter (LDSE) processing, allowing simultaneous ARC removal and deep emitter formation. However, the technology did not make it into the market so far. Adhesion issues have been speculated to be a major drawback.

Hence the most important goal for successful industrial implementation of this metallization scheme is to reliably achieve sufficient adhesion for module integration while maintaining high cell efficiency and low process complexity. Two major process routes are currently propagated to achieve this goal:

Silicides formed from evaporated or sputtered metal layers for contacts on collector, base and emitter form the current state of the art connections in VLSI devices [11] and nickel silicide has developed to be the contact material of choice due to a low thermal budget for formation, low resistivity and low Si consumption [12]. In the so called "salicide" process, silicide is formed from a thin layer of evaporated or sputtered metal, excess metal is etched away and conductor tracks are deposited on top of the silicide [11]. For PV applications adhesion promotion by silicide formation is postulated by a number of publications in PV [1], [3], [5], [9], [13]–[15] and excellent adhesion has been shown after specific treatment in a previous publication [16]. The mentioned CMOS process for silicide contacts was employed as a guideline within said publication. The first process route followed in this paper features ps-laser ablation followed by a plating sequence close to this procedure with interim thermal silicidation after nickel deposition. The second process sequence is a simplified route of full stack plating and post anneal [4].

2 EXPERIMENTAL

Different cell concepts may be metallized by plating and only a few ones are shown here. These are standard BSF-cells, n-Type BSF cells and n-Type *PassDop* cells. Different patterning technologies have come into play. Their fabrication and characterization methods are shown in the following.

2.1 Cell manufacturing

Cz Si wafers were treated by a standard industrial front end for solar cells, consisting of the following: Damage etching, alkaline texturing, PSG removal, $POCl_3$ emitter diffusion, single sided emitter etchback, SiN_X PECVD (plasma enhanced chemical vapour deposition), rear side full area screen printing of Al paste with Ag

soldering pads and firing. This process sequence resulted in standard BSF cells without front side metallization with an emitter of 90 Ω/sq.
Different ARC patterning technologies have been examined in terms of resulting Si surface roughness. In the ‘Mask & Etch’ process a mask is applied either by photolithographic methods or via inkjet printing. The mask leaves the ARC uncovered in grid pattern, which is removed by chemical etching in these openings.
Laser ablation of the ARC has been applied with help of a ns-laser or a ps-laser, both with a wavelength of 355 nm [17]. The ablation process is classified indirect, since UV irradiation passes the ARC and a thin layer of underlying Si is evaporated, which causes the ARC to be blast away. The longer pulse duration of the ns laser allows a larger volume to be molten and a may result in remodelling of the surface texture and the emitter. The short duration of a ps-pulse causes minimum emitter damage and the effects of interference of light, reflected from the pyramid flanks translates into surface remodelling on a nano scale. During laser chemical processing (LCP) a laser beam is coupled into a liquid jet, which may contain different chemicals, such as a dopant source. This is used for simultaneous formation of a selective emitter during ARC patterning [18]. Surface remodelling is possible on a similar scale as ns-laser processes, yet emitter damage is avoided and higher laser power may be tolerated.

The two different process routes for metallization, featuring ps-laser patterning, are shown in the flow chart in Fig. 1. Both apply the same front end up to the deposition of the anti-reflection coating (ARC) followed by laser patterning. For most experiments, an industrial laser ablation tool with a mounted ps-laser system was used. For demonstration purposes, a lab setup optimized for very small line widths was used in one experiment.

The first route utilizes nickel silicides as bonding agent. In microelectronics silicides are formed from evaporated or sputtered Ni. A wafer surface is masked by a patterned SiO_X layer and silicidation only occurs in exposed areas. This method was taken as a model and adapted for solar cell metallization. After pretreatment the first route consisted of deposition of an extremely thin Ni layer, which was fully consumed during subsequent thermal silicidation. After pretreatment of the silicide surface the full stack of Ni, Cu and Ag was deposited. This will be named “Interim Annealing” route in the following.
The second process route consisted of full stack deposition of Ni, Cu and Ag and subsequent thermal annealing in forming gas atmosphere. This will be named “Post Anneal” route in the following.

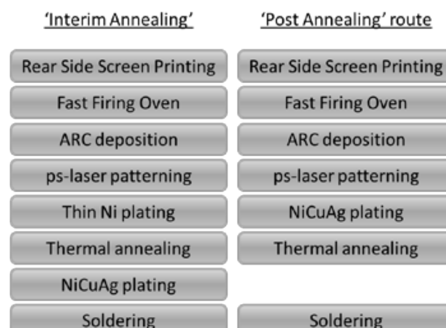

Fig. 1: Process flow chart of the two different routes

The process sequences for efficiency potential demonstration of NiCu contacts on next generation solar cell concepts are described elsewhere, being [19] for n-type BSF cells and [20] for n-type *PassDop* cells.

2.2 Plating Processes and Tools

Pretreatment and metal deposition was performed in industrial inline machines for single sided processing, RENA InCellPlate. Pretreatment was done 1% HF solution for removal of native oxide of the Si surface. A displacement electrolyte was used for minimum Ni layer thickness deposition [21]. A Watt’s type electrolyte was used for Ni deposition of diffusion barrier layers, which is described elsewhere [1]. A low pH electrolyte based on sulphuric acid was used for Cu deposition, a cyanide-free electrolyte for Ag capping layers.

2.3 Characterization

3D colour imaging was done with help of an Olympus OLS4000 laser microscope and SEM imaging was performed with help of either a Hitachi SU-70 or a Zeiss Auriga60. The metal adhesive strength was measured on the BSF cells only, as these are the ones with suitable size for testing. Results may be transferred to next generation cell concepts because of comparable surface situations. Adhesive strength was measured by a tensile testing machine from Frolyt. The test is similar to the procedure in DIN EN 28510-1, but is not certified or calibrated. One end of the cell ribbon is clamped to the testing machine, while the cell is mounted in a hold-down unit. The cell ribbon is peeled with a constant speed of 1 mm/s at a constant angle of 90° between ribbon and cell. For comparison a test measurement has also been performed at 45° angle.

3 RESULTS AND DISCUSSION

3.1 Evaluation of peel force measurements and their relation to adhesive force between metal and silicon

Details to the peel force measurement procedure of soldered joints in solar modules are defined in IEC 61189-2 and according to DIN EN 50461, the peel force requirement is set to 1 N/mm of busbar width. Yet the module construction community neither fully agrees on minimum required adhesive strength for module construction, nor on measurement details itself. A discussion has arisen, if these definitions are rational, since modules have been successfully constructed with cells, not fully meeting these requirements. Different institutions have published results from alternative measurement procedures and some confusion has come up with this practice. Some publications apply measurements at different angles, such as 45°, 135° or 180° and some do not mention the angle at all, while the standard defines $(90 \pm 5)°$ degrees at a peeling speed of (50 ± 5) mm/min. A very good consideration of the topic is given in [22], showing that 45° peel angle induced least stress on the metallization, 90° and 180° are comparable and highest stress onto the metal-silicon interface is induced at 135°. A comparison of peel force measurements at 45° and 90° angle of two solar cells of medium metal adhesive strength, which were identically metallized, is shown in Fig. 2. Differences in peel force agree with considerations from [22].

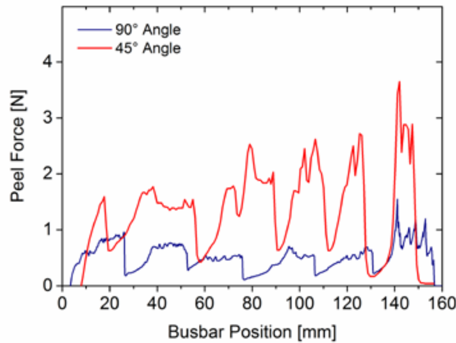

Fig. 2: Peel force diagram, comparing 45° and 90° peeling angle for identically processed metallization, with six individual automated solder spots on a 1.5 mm busbar

While the measured peel force is consistent for the solder spots in the 90° angle measurement, the measured peel force rises throughout the measurement by angle change for the 45° angle measurement and shows up to three times higher force, which exceeds wafer breakage force. We have concluded to set the peeling angle to 90° for all following measurements.

A further confusion has arisen about stated numerical values. Some publications list the lowest, some the highest, some an average value and some don't mention how a stated value is derived [4], [7], [23]. According to IEC 61189-2 the lowest value during measurement is to be listed in N/mm. Also according to the standard, the metal is to be peeled off. Yet for very high metal adhesive strength, silicon wafer breakage is observed, rather than true metal peeling to occur. During measurement Si slabs in the size of up to a cm may break out. In the moment of fracture the highest force is recorded and peaks are plotted in peel force diagrams. Their height depends on wafer breakage force, which again depends on wafer quality, thickness, treatment and supporting layers such as the Al rear side metallization. This is followed by a dip in the curve during straightening of the solder ribbon before the position of the next wafer fracture. The dip size depends on slab size. For busbars of different width below the size of these Si slabs a very similar wafer breakage force is recorded. Yet the standard demands the statement of a value in the unit N/mm, hence any value would need to be divided by the busbar width which would lead to a large error. For instance a busbar with 2 mm width would be declared to have half the adhesive force than a busbar with 1 mm width. Also fractures are continued along cleavage tendency and promote further fracturing during pee force measurement.

According to IEC 61189-2 a test specimen with a thickness below 0.8 mm is to be fortified, e.g. by gluing it to a rigid piece of material. Si solar cells obviously do not meet this thickness requirement, since the used wafers usually lie below 200 µm thickness. Peel force diagrams of NiCu metallization following the "Interim Anneal" process route are compared with an identically processed cell, of which the back side had been glued to a brass sheet of 1 mm thickness (see Fig. 3). The applied glue was a two component epoxy adhesive of the make Loctite Hysol® 3425.

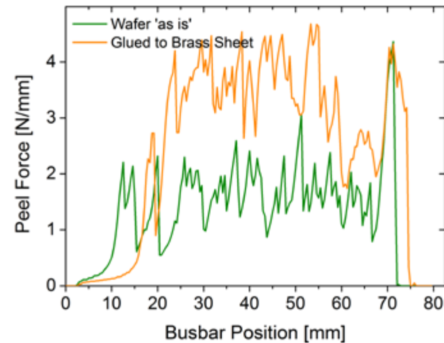

Fig. 3: Peel force diagram of a clamped and a fortified wafer, comparing identically processed metallization of highest adhesive strength, following the "Interim Anneal" process sequence after Mask & Etch ARC patterning on a 1 mm busbar

In case of a fortified wafer only small Si chunks in size of up to one mm are ripped out of the wafer surface, which requires a larger force than for an unfortified wafer. Although the true adhesive strength is virtually the same, roughly double the force is measured. In both cases the true metal adhesive strength is higher than wafer breakage force. Since breakage force corresponds to the peaks in the diagrams, an adhesive strength above this force may be reported.

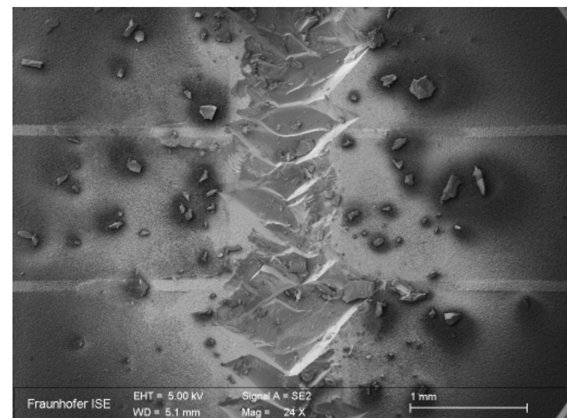

Fig. 4: SEM image of a busbar from a Mask & Etch cell after peel force measurement with adhesive forces above 4.5 N/mm

In case of true metal peeling without Si breakage a similar mechanism is observed. During uniform movement of the peel force testing machine a jerky progression of the peeling interface is observed. The recorded peaks may be seen as peeling of metal patches and during subsequent dips the tension in the pulled ribbon rises until enough force for next patch to peel is reached. Here also the peaks can be referred to, yet in this case obviously as the *true* peel force.

Regarding the specimen thickness and the value to be considered as peel force (lowest / highest value in peel force diagram) these observations put the definition of the IEC standard into question for application on solar cells and an adaptation is recommended. Listing peak forces is rational while two cases need to be distinguished. True metal peeling and rip-outs, for which a strength greater than measured may be stated. The

breakage force of Si wafers is typically above the required 1 N/mm from DIN EN 50461 and for practical reason it may be reasonable to omit the effort of wafer fortification and state the adhesive force to be greater than measured peak forces.

3.2 Adhesion promotion and electrical results

For the "Interim Anneal" route adhesion results have already been shown in Fig. 3. Plated metal on the silicide bonding agent reliably shows excellent adhesive strength independent from surface roughness. The shown results are for Mask & Etch ARC patterning, which typically shows the lowest initial adhesion due to a very smooth surface. Yet silicide thickness needs to be kept well below emitter thickness, otherwise leakage current or even emitter shunting may occur, which would lead to performance degradation (j_{02} increase, pFF decrease). Silicide thickness may be limited by mild annealing conditions or by limiting the diffusion source – meaning the thickness of the deposited Ni layer. The latter is inherently not possible for the "Post Anneal" route as sufficient nickel needs to be plated to hinder copper diffusion effectively.

Process steps were minimized for this route by minimum Ni deposition thickness for full Ni consumption during silicidation. Hence, compared to the process from [16], the selective Ni etchback was omitted and penetration depth was limited by limiting the Ni source.

For minimum shading by the metallization, grid lines are aimed to be a small as possible, yet sufficiently conductive. After standard ps-laser ablation in an industrial type machine and plating of the stack of NiCuAg/Sn a seed layer width of 21.5 µm and a line width as low as 42 µm was reached (see Fig. 5 (left)). Optimized lab type laser ablation, which also may easily be implemented in industrial machines, even led to a finger width of 20 µm (see Fig. 5 (right)).

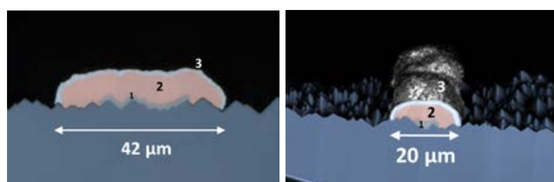

Fig. 5: Optical microscope images of cross sections of plated NiCuAg Fingers after industrial type laser ablation (left) and optimized lab laser process (right), labels 1 for Ni seed layer, 2 for Cu layer and 3 for capping layer

A dependence of Si surface roughness to adhesive force of plated Ni was found. In Fig. 6 different surface roughnesses are shown, as a result of different treatments. The image top-left shows a typically smooth Si surface, after chemical etching of the ARC - within the border to the remaining ARC is shown. The top-right image shows the surface roughness which results from ns-laser ablation with a set power high enough for surface modification with the risk of emitter damage. The bottom-left image shows a Si surface after laser-chemical processing with a laser power set to modify the surface texture to a certain degree. The bottom-right image shows the Si surface after ps-laser ablation, where interference patterns on a nano-scale are visible.

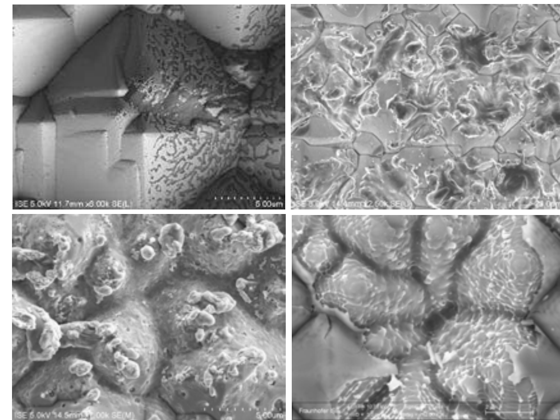

Fig. 6: SEM images, displaying the surface roughness resulting from chemical ARC etching (top-left), high power ns-laser ablation (top-right), laser chemical processing (bottom-left and ps-laser ablation (bottom-right)

The patterns are caused by interference of the primary beam with light, reflected from the pyramid flanks and of reflected light with reflected light from a different pyramid flank [24]. The size of the interference patterns depends on wavelength and therefore there are pits and bridge-like features in a distance of 355 nm from one another.

The effect of the respective resulting surface roughness on metal adhesion has been compared, utilizing the "Post Anneal" route. A Peel force diagram can be seen in Fig. 7, which shows increasing metal adhesive strength with increasing surface roughness, resulting from ARC patterning method.

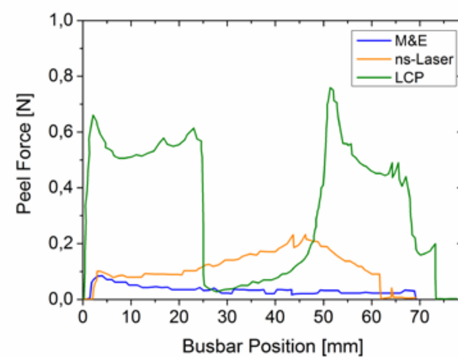

Fig. 7: Peel force diagram of plated NiCu metallization on three different surfaces of low roughness and resulting unreliable and insufficient adhesion, thereby LCP stands for 'laser chemical processing' and M&E for 'Mask and Etch'

Wet chemical etching results in the smoothest surfaces, leading to peel forces constantly staying below 0.1 N/mm. (Note the drastically higher peel force for cells with the same ablation technique, featuring silicide as adhesion promoter, Fig. 3.) The plated metal on ns laser ablated busbars shows a higher adhesive force, yet of inconsistent and insufficient value. ARC ablation by LCP may lead to relatively high roughness and higher adhesion values, yet still below the requirement of the IEC and of unreliable impression. For ps laser ablation, adhesion is close to the required value even without thermal annealing. Highest peel force is measured for the cells featuring ps laser ablation and thermal annealing, of

which a peel force diagram is shown in Fig. 8.

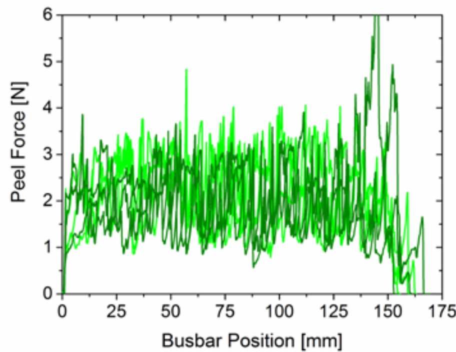

Fig. 8: Peel force diagram of multiple measurements of cells produced following the "Post Anneal" route with 1.5 mm busbars, showing excellent adhesion

Resulting measurements of solar cell efficiency for different sample types are listed in Table I. All cells feature a high fill factor, which demonstrates the capability of the plated metallization to contact both standard cells and alternative cell concepts. The *PassDop* cell result shows that the plated metallization may contact boron emitters with low resistivity while avoiding voltage loss.

Table I: IV measurement results for different concepts featuring NiCu contacts

Cell Type	Jsc [mA/cm^2]	Voc [mV]	FF [%]	η [%]
Standard BSF "Interim"	37.84	639.5	79.6	19.3
Standard BSF "Post Anneal"	37.93	640.5	80.0	19.4
n-Type BSF "Interim"	38.27	655.3	81.8	20.5
n-Type *PassDop* "Interim"	40.01	678.2	81.3	22.1

4 CONCLUSIONS

Fully plated NiCu contacts are indeed suitable for high efficiency industrial and next generation solar cells. High efficiency solar cells have been demonstrated on different cell structures. Excellent metal adhesion is created by thermal formation of a nickel silicide bonding agent from a plated Ni layer, independent of the surface roughness. A thin Ni layer may be deposited, resulting in full Ni consumption and thereby omitting a process step and reducing the fabrication cost of the sequence.

With rising surface roughness the metal adhesion is promoted even without silicide formation. The highest adhesion is found for ps-laser ablation. This may be a result of the scale of topological features, their uniformity and distribution. It also may be a result from interlocking of plated metal into opposite lying structures, as schematically shown in Fig. 9. Facing flanks of neighbouring pyramids allow direct interlocking of plated metal by the topological features. These features on opposing outer pyramid flanks also keep the plated metal immobile and thereby potentially even be feasible without thermal annealing.

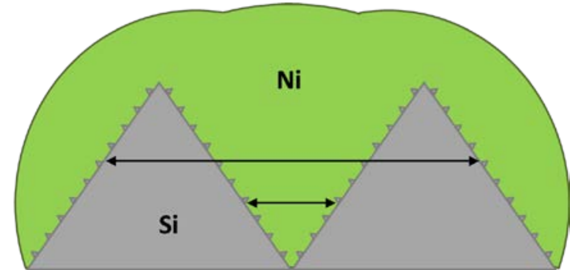

Fig. 9: Schematic cross section view of Si texture pyramids with increased surface roughness by ps-laser ablation and plated Ni. The arrows are pointing at interlocking positions between facing neighbouring pyramid flanks and opposing outer flanks of neighbouring pyramids

The "Interim Annealing" route basically has 2-4 m longer wet chemical equipment for an inline machine, yet it might be more suited for highest efficiency emitters, since it offers low contact resistance to even very low surface dopant concentrations due to different effects, such as the so-called snowplough-effect [25] and beneficial barrier height [26]. As demonstrated on Mask & Etch cells, it is independent from surface roughness (compare Fig. 3).

Both routes lead to excellent adhesion and may be considered, depending on convenience and compatible processes in the process sequence of different solar cell concepts.

ACKNOWLEDGEMENTS

The authors want to thank Gisela Cimiotti for chemical laboratory work and plating processes, Matthias Weng for annealing operations and Alexander Maier for soldering and peel force measurements. This work was funded by the German Federal Ministry for the Environment, Nature Conservation and Nuclear Safety (Contract Number 0325187).

REFERENCES

[1] J. Bartsch, "Advanced Front Side Metallization for Crystalline Silicon Solar Cells with Electrochemical Techniques," PhD Thesis, Albert-Ludwigs-Universität, 2011.

[2] P. Cousins and D. Smith, "Generation 3: Improved performance at lower cost," *Photovolt. Spec. Conf. (PVSC), 2010 35th IEEE*, 2010.

[3] A. Lennon, Y. Yao, and S. Wenham, "Evolution of metal plating for silicon solar cell metallisation," *Prog. Photovoltaics …*, no. May 2012, pp. 1454–1468, 2013.

[4] R. Russell, L. Tous, H. Philipsen, J. Horzel, E. Cornagliotti, M. Ngamo, P. Choulat, R. Labie, J. Beckers, J. Bertens, M. Fujii, J. John, J. Poortmans, and R. Mertens, "A simple copper metallisation process for high cell efficiencies and reliable modules," in *27th European Photovoltaic Solar Energy Conference and Exhibition*, 2012.

[5] N. Mason, D. Jordan, and J. Summers, "A high efficiency silicon solar cell production technology," in *Tenth EC Photovoltaic Solar Energy Conference*, 1991.

[6] A. Mette, "New Concepts for Front Side Metallization of Industrial Silicon Solar Cells," 2007.

[7] L. Tous, R. Russell, J. Das, R. Labie, M. Ngamo, J. Horzel, H. Philipsen, J. Sniekers, K. Vandermissen, L. van den Brekel, T. Janssens, M. Aleman, D. H. van Dorp, J. Poortmans, and R. Mertens, "Large Area Copper Plated Silicon Solar Cell Exceeding 19.5% Efficiency," *Energy Procedia*, vol. 21, no. October 2011, pp. 58–65, Jan. 2012.

[8] J. Zhao, A. Wang, and P. Altermatt, "24% efficient PERL silicon solar cell: recent improvements in high efficiency silicon cell research," *Sol. Energy Mater. Sol. Cells Mater. Sol. cells*, vol. 42, pp. 87–99, 1996.

[9] A. Mondon, J. Bartsch, B. J. Godejohann, M. Hörteis, and S. W. Glunz, "Advanced Front Side Meltallization for Crystalline Silicon Solar Cells Based on a Nickel-Silicon Contact," in *2nd Workshop on Metallization for Crystalline Silicon Solar Cells*, 2010, pp. 42–47.

[10] Z. Shi, S. Wenham, and J. Ji, "Mass production of the innovative PLUTO solar cell technology," *2009 34th IEEE Photovolt. Spec. Conf.*, pp. 001922–001926, Jun. 2009.

[11] R. W. Mann, L. A. Clevenger, P. D. Agnello, and F. R. White, "Silicides and local interconnections for high-performance VLSI applications," *IBM J. Res. Dev.*, vol. 39, no. 4, pp. 403–417, 1995.

[12] C. Lavoie, F. M. d'Heurle, C. Detavernier, and C. Cabral, "Towards implementation of a nickel silicide process for CMOS technologies," *Microelectron. Eng.*, vol. 70, no. 2–4, pp. 144–157, Nov. 2003.

[13] C. Dheasuna, "Novel buried contact technology for advanced silicon solar cells," *First WCPEC*, 1994.

[14] L. Tous, J. Lerat, and T. Emeraud, "Nickel silicide contacts formed by excimer laser annealing for high efficiency solar cells," *Prog. Photovoltaics Res. Appl.*, no. January, pp. 267–275, 2013.

[15] Z. Hameiri, L. Mai, and S. Wenham, "Advantages of photoplating for laser doped solar cells," *Prog. Photovoltaics Res. Appl.*, pp. 511–516, 2011.

[16] A. Mondon, M. N. Jawaid, J. Bartsch, M. Glatthaar, and S. W. Glunz, "Microstructure analysis of the interface situation and adhesion of thermally formed nickel silicide for plated nickel–copper contacts on silicon solar cells," *Sol. Energy Mater. Sol. Cells*, vol. 117, pp. 209–213, Oct. 2013.

[17] A. Brand and A. Knorz, "Nanosecond laser annealing to decrease the damage of picosecond laser ablation of anti-reflection layers on textured silicon surfaces," in *Proc. SPIE, Laser Material Processing for Solar Energy, 84730D*, 2012, no. March.

[18] D. Kray, a. Fell, S. Hopman, K. Mayer, G. P. Willeke, and S. W. Glunz, "Laser Chemical Processing (LCP)—A versatile tool for microstructuring applications," *Appl. Phys. A*, vol. 93, no. 1, pp. 99–103, Jul. 2008.

[19] A. Richter, J. Benick, A. Kalio, J. Seiffe, M. Hörteis, M. Hermle, and S. W. Glunz, "Towards industrial n-type PERT silicon solar cells: rear passivation and metallization scheme," *Energy Procedia*, vol. 8, pp. 479–486, Jan. 2011.

[20] B. Steinhauser, M. Bin Mansoor, U. Jäger, J. Benick, and M. Hermle, "Firing-stable PassDop passivation for screen printed n-type PERL solar cells based on a-SiNx:P," *Sol. Energy Mater. Sol. Cells*, vol. 126, pp. 96–100, Jul. 2014.

[21] F. a. Harraz, T. Sakka, and Y. H. Ogata, "Immersion plating of nickel onto a porous silicon layer from fluoride solutions," *Phys. Status Solidi*, vol. 197, no. 1, pp. 51–56, May 2003.

[22] U. Eitner and L. C. Rendler, "The Mechanical Theory Behind the Peel Test," in *SiliconPV 2014*, 2014, vol. 00, pp. 0–4.

[23] B. Tjahjono, M. Yang, C. Lan, and J. Ting, "18.9% efficient laser doped selective emitter solar cell on industrial grade p-type czochralski wafer," in *25th European Photovoltaic Solar Energy Conference and Exhibition*, 2010, no. September 2010, pp. 6–10.

[24] A. Knorz, M. Peters, A. Grohe, C. Harmel, and R. Preu, "Selective laser ablation of SiNx layers on textured surfaces for low temperature front side metallizations," *Prog. Photovoltaics Res. Appl.*, no. October, pp. 127–136, 2009.

[25] T. Morimoto and T. Ohguro, "Self-aligned nickel-mono-silicide technology for high-speed deep submicrometer logic CMOS ULSI," *Electron Devices, …*, vol. 42, no. 5, 1995.

[26] K. Maex and M. Van Rossum, *Properties of Metal Silicides*, 1st ed. Leuven, Belgium: INSPEC, the Institution of Electrical Engineers, 1995.